Materials Advances

ROYAL SOCIETY OF CHEMISTRY

PAPER

View Article Online
View Journal

Cite this: DOI: 10.1039/d6ma00154h

DFT insights into heteroatom-doped C_{60} nanocages as potential drug carriers for lorazepam

Mariam M. Seliem, †[a] Mohamed M. Aboelnga, †*[ab] Elsayed El-Bayoumy [a] and Mohsen El-Tahawy *[c]

Efficient delivery of lorazepam remains challenging due to its poor aqueous solubility, limited bioavailability, and delayed onset of action. In this work, a density functional theory (DFT) study was conducted to investigate the adsorption behavior of lorazepam on pristine C_{60}, SiC_{59}, and GeC_{59} nanostructures as potential drug delivery systems. Various adsorption configurations were optimized to identify the most stable binding modes and interaction mechanisms. The calculated adsorption energies indicate that C_{60} exhibits relatively weaker interactions compared to doped systems, while silicon and germanium doping significantly enhance the adsorption strength. In particular, the SiC_{59} system shows the highest stability, with adsorption energies reaching approximately −6.1 eV, indicating strong binding suitable for drug loading applications. GeC_{59} also demonstrates enhanced adsorption compared to C_{60}, although weaker than Si doping. Several analytical tools were employed, including reduced density gradient (RDG–NCI) analysis, partial density of states (PDOS), natural bond orbital (NBO) analysis, infrared (IR) spectroscopy, work function (φ), and HOMO–LUMO gap, which confirm significant electronic interaction and charge transfer between the drug and nanocarrier. Solvent effects further reveal that adsorption remains energetically favorable in aqueous environments. Importantly, protonation studies under acidic conditions demonstrate a significant weakening of the interaction, confirming the feasibility of a pH-responsive drug release mechanism. Overall, these findings highlight doped C_{60} nanocages, especially SiC_{59}, as promising candidates for efficient and controlled lorazepam delivery.

Received 2nd February 2026,
Accepted 4th May 2026

DOI: 10.1039/d6ma00154h

rsc.li/materials-advances

1. Introduction

Efficient drug delivery remains one of the most significant challenges in achieving optimal therapeutic efficacy for treating various diseases and viral infections. Despite significant advances in pharmacology and formulation development, conventional drug administration routes continue to face major biopharmaceutical limitations, including poor aqueous solubility, limited permeability across biological membranes, and low bioavailability. These drawbacks often result in reduced therapeutic efficacy and unpredictable pharmacokinetics.[1] Moreover, systemic distribution of drugs without targeting mechanisms can lead to nonspecific accumulation in healthy tissues and undesirable side effects, particularly in treatments requiring high drug concentrations for efficacy.[2–4]

To overcome these limitations, nanotechnology has emerged as a promising strategy for developing advanced drug delivery systems (DDSs) capable of improving drug solubility, stability, and targeted delivery while minimizing systemic toxicity.[5,6]

Among clinically important therapeutic agents, lorazepam, a benzodiazepine derivative, is widely used for its anxiolytic and sedative properties but suffers from several delivery related limitations. These include its low aqueous solubility ($\sim$0.08 mg mL^{-1}),[7] poor chemical stability,[8] and delayed onset of action following oral administration.[9–11] Such limitations can lead to suboptimal therapeutic outcomes and increase the risk of overdose due to delayed pharmacological response. Consequently, developing alternative delivery strategies for lorazepam is essential to enhance its clinical performance.

In this context, adsorption of lorazepam onto suitable nanocarriers represents a promising strategy to improve its solubility, stability, and delivery efficiency. Carbon-based nanostructures, such as fullerenes, carbon nanotubes, and

[a] Chemistry Department, Faculty of Science, Damietta University, 34511 Damietta, Egypt. E-mail: mariamseliem@students.du.edu.eg, mohamed-aboelnga@du.edu.eg, sayedelbayoumy@du.edu.eg
[b] King Salman International University, Faculty of Basic Sciences, Ras Sudr 46612, South Sinai, Egypt
[c] Chemistry Department, Faculty of Science, Damanhour University, 22511 Damanhour, Egypt. E-mail: mohsen.eltahawy@sci.dmu.edu.eg
† These authors contributed equally to this work.

graphene, have attracted considerable attention as potential drug carriers due to their unique physicochemical properties, including high surface area, tunable electronic characteristics, and favorable biocompatibility.[12–14] These properties facilitate strong interactions with drug molecules, enabling improved drug loading, stability, and controlled release behavior.

Among carbon nanomaterials, fullerene C_{60} has emerged as a particularly attractive nanocarrier owing to its spherical geometry, high symmetry, and electron-accepting ability.[15] The π-conjugated cage-like structure of C_{60}, composed of 60 carbon atoms, provides an extensive surface area that promotes efficient interaction with therapeutic molecules, primarily through chemisorptive mechanisms.[16,17] Previous theoretical and experimental studies have demonstrated that fullerenes can form stable complexes with a wide range of drugs, leading to enhanced pharmacokinetic properties and prolonged circulation times.[16]

To gain molecular level insight into these interactions, DFT has been widely employed as a reliable computational approach for studying drug–nanocarrier systems. DFT enables detailed analysis of adsorption energies, charge transfer, electronic structure modifications, and interaction mechanisms, offering valuable information for the rational design of nanocarrier-based DDSs.[18–20]

Furthermore, the adsorption performance and electronic properties of fullerene surfaces can be significantly enhanced through heteroatom doping. Incorporation of dopant atoms such as silicon (Si) and germanium (Ge) introduces localized electronic density variations, creates new active adsorption sites, and improves charge transfer between the drug molecule and the nanocarrier.[21–23]

Silicon doping has been reported to enhance the thermal and mechanical stability of C_{60} while increasing the number of active binding sites and modifying the band gap, thereby improving sensitivity to photoreactions and molecular interactions.[24–32] Similarly, germanium doping, owing to its larger atomic radius and higher polarizability, further enhances surface reactivity and adsorption stability, making it particularly advantageous for drug delivery applications involving lorazepam.[33–35] In addition to elemental doping, various surface modification and functionalization strategies have been explored to improve the delivery efficiency and controlled release behavior of fullerene-based carriers. For instance, PEG-functionalized iron-encapsulated C_{60} (Fe@C_{60}:PEG) has shown enhanced stability and dipole moment, leading to improved adsorption energetics for anticancer drugs such as carboplatin.[36] Alkali metal decoration (Li, Na, K) of C_{60} has also been demonstrated to generate multiple active sites capable of carrying several drug molecules, such as 5-fluorouracil, while maintaining reversible adsorption suitable for controlled release under physiological conditions.[37] Additionally, transition metal-doped fullerenes (*e.g.*, Cr, Fe, Ni) have exhibited enhanced adsorption and charge transfer interactions with antiviral drugs, suggesting improved delivery performance in aqueous biological environments.[38] Experimental studies further support the potential of fullerene-based DDSs. Complexes of C_{60} with anticancer drugs, such as doxorubicin, have demonstrated enhanced cytotoxicity and improved antitumor efficacy *in vivo* compared to the free drug, highlighting the ability of fullerene carriers to improve drug accumulation at target sites and modulate biological responses.[39] Moreover, C_{60} nanocomplexes have been shown to influence immune cell activity and oxidative stress pathways, indicating potential synergistic therapeutic effects beyond conventional drug transport.[40]

Based on these findings, the present study employs DFT to systematically investigate and compare the adsorption behavior of lorazepam on pristine fullerene C_{60}, silicon-doped fullerene, and germanium-doped fullerene. Multiple adsorption configurations, from configuration (1) to configuration (5), were optimized and analyzed. Electronic structure properties were examined through partial density of states (PDOS) and HOMO–LUMO analysis to elucidate the charge transfer mechanisms and adsorption stability.[15,41] Vibrational properties were explored using IR spectroscopy to identify characteristic frequency shifts and distinguish between physisorption and chemisorption interactions.[42] Additionally, RDG–NCI and NBO analyses, along with thermodynamic parameters (ΔG, ΔH, and ΔS), were evaluated to obtain comprehensive insight into the interaction mechanisms and feasibility of these systems.[33,43–46] The work function and solvent effects in aqueous environments were also assessed to evaluate the practical applicability of these nanocarriers in biological systems. Furthermore, to assess the potential for controlled drug release, the effect of protonation under acidic conditions (pH < 7) on the interaction strength was also investigated for config. (1) of SiC_{59}, demonstrating that the drug–nanocarrier complexes maintain strong and stable interactions without any loss of adsorption efficiency.

2. Computational methods

DFT calculations were used to investigate the adsorption behavior of lorazepam onto both pristine and metal-doped fullerene surfaces in gaseous and aqueous phases. These calculations allowed for the prediction of adsorption mechanisms through the determination of molecular descriptors and adsorption energies, specifically by evaluating the binding energy between the lorazepam drug and fullerene. Geometry optimizations and electronic characteristics for all the studied complexes and different binding orientations were performed using the Gaussian 16 software on both pristine fullerene and metal-doped fullerene,[47,48] where the system was modeled as a finite molecular cluster.[49,50] Fullerene C_{60} is a spherical molecule composed of sixty carbon atoms arranged in a hollow cage structure resembling a soccer ball. Its geometry consists of twelve pentagonal and twenty hexagonal carbon rings that are interconnected, giving the molecule a highly symmetrical shape. Because the carbon atoms are distributed in all three spatial directions, C_{60} is classified as a three-dimensional (3D) form of carbon. This distinguishes it from materials like

graphene, which is two-dimensional since its atoms lie on a single plane, and from carbon nanotubes, which are one-dimensional. The closed, cage-like structure of fullerene provides it with a definite volume in space, making it one of the most fascinating 3D allotropes of carbon, alongside diamond.

The B3LYP functional with Grimme's dispersion correction (B3LYP-D3) was employed in this study, as it is one of the most extensively used and well-validated functionals in the literature for investigating molecular adsorption on carbon-based nanostructures,[43,51] offering a reliable balance between accuracy and computational efficiency. As a methodological validation, selected complexes were re-optimized using the 6-31+G(d) basis set and with the ωB97XD functional to validate the reliability of the chosen level of theory, revealing that the adsorption orientations and interaction sites remain unchanged, with no significant structural rearrangement; the detailed comparison is provided in the supplementary information (SI, Fig. S8 in pages 8–9). This combination has been successfully employed to represent various chemical systems.[52–56] The standard 6-31G(d) basis set was applied to ensure a suitable balance between computational cost and accuracy, and has been widely used for fullerene–drug interaction studies.[57–59] DFT enabled the identification of potential adsorption sites and the characterization of drug–surface interactions, including chemisorptive bonding.[60] In this study, all geometries were re-optimized in the solvent environment, by accounting for solvent effects, and the integral equation formalism polarizable continuum model (IEFPCM) was employed, simulating water as the solvent.[61–64] Water was considered as a basic approximation to represent solvent effects; however, it is acknowledged that real physiological environments contain various ions, biomolecules, and other competing species that may influence the interactions. This approach allowed us to evaluate the influence of the aqueous environment on the adsorption behavior and electronic properties of the lorazepam drug on pristine and doped fullerene surfaces. Frequency calculations confirmed that all optimized structures correspond to true minima on the potential energy surface, with no imaginary frequencies detected. Partial density of states (PDOS) calculations were carried out for the optimized lorazepam–fullerene complexes in the vacuum phase to analyze the orbital contributions of the drug and the surface to the interfacial electronic structure. In contrast, total density of states (DOS) calculations were performed for the solvated systems to assess solvent-induced modifications in the overall electronic structure. The molecular structures and the electronic properties, including the highest occupied molecular orbits (HOMO) and lowest unoccupied molecular orbits (LUMO) have been analyzed and visualized utilizing GaussView 6.0. To explore intermolecular interactions, visual molecular dynamics (VMD),[65] Gnuplot,[66] and natural bond orbital (NBO) analysis were performed on the obtained C_{60}–lorazepam drug complexes, employing the same level of theory and basis set,[67] and Multiwfn software[68] was employed for generating RDG plots and NCI iso-surfaces. DOS, PDOS and IR spectra were analyzed utilizing GaussSum software.[69] The binding energy (E_{bind}) is defined as the following:

$$E_{bind} = E_{C_{60}\backslash lorazepam\ drug} - (E_{lorazepam\ drug} + E_{C_{60}}) \quad (1)$$

Here, $E_{lorazepam\ drug}$ represents the energy of the lorazepam drug, $E_{C_{60}}$ is the energy of the fullerene, and $E_{C_{60}\backslash lorazepam\ drug}$ is the energy of the fullerene after interacting with drug molecules to form the corresponding complexes with different orientations, where the negative adsorption energies indicate that the complexation process is exothermic.

The HOMO–LUMO energy gap (E_{gap}) is estimated by the difference between the HOMO' energy (E_H) and LUMO energy (E_L),[70] which is expressed as follows:

$$E_{gap} = E_L - E_H \quad (2)$$

where a large E_{gap} signifies chemically hard molecules that interact weakly with other systems; in contrast, a moderate E_{gap} enhances reactivity by facilitating favorable HOMO–LUMO interactions in chemical processes.

$$E_F = (E_{LUMO} + E_{HOMO})/2 \quad (3)$$

where E_{LUMO} and E_{HOMO} represent the energies of the LUMO and HOMO, respectively.

To evaluate solvent effects, the integral equation formalism polarizable continuum model (IEFPCM)[71] has been employed using H_2O as a solvent phase. The solvation energy (E_{sol}) was obtained according to the following equation;[72]

$$E_{sol} = E_{water} - E_{gas} \quad (4)$$

where E_{water} and E_{gas} represent the total energies of the complexes in the aqueous and gas phases, respectively. To verify the reliability and stability of the optimized structures, thermodynamic parameters such as Gibbs free energy (ΔG), enthalpy (ΔH), and entropy (ΔS) were computed.

3. Results and discussion

Initially, five different adsorption configurations were examined for the interaction of the lorazepam molecule with pristine–C_{60} surfaces. Among these models, the two most stable configurations (1) and (5) were selected, which are shown in Fig. 1. This investigation has been further expanded using several analytical tools, such as RDG-NCI analysis, PDOS, IR spectroscopy, NBO analysis and HOMO–LUMO gap analysis, to gain a comprehensive understanding of the molecular interactions and behavior.

In this study, the two most stable adsorption configurations, (1) and (5), were selected based on their highest binding energy values. These two complexes were further modified by doping the C_{60} surface with Si and Ge atoms. The details of the doped systems and their comparative analysis will be discussed in the following sections.

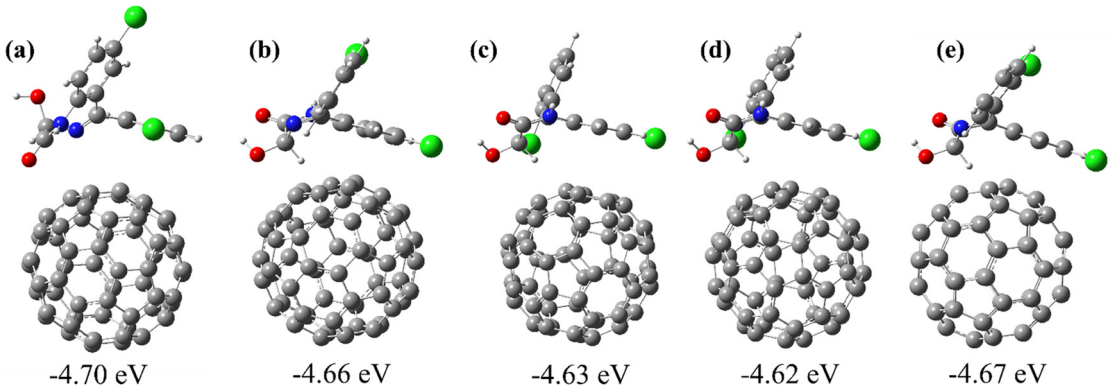

Fig. 1 The optimized geometries of lorazepam adsorbed on C_{60} fullerenes of different orientations (1) to (5) are represented as (a)–(e) with their binding energy, respectively.

3.1. Molecular insights into lorazepam drug adsorption on C_{60}

The adsorption behavior of lorazepam on the C_{60} fullerene surface was examined through geometric optimization, electron density analysis, vibrational assessment, and electronic structure calculations. Among the explored orientations, configurations (1) and (5) were identified as the most stable, exhibiting adsorption energies of −4.70 eV and −4.67 eV, respectively. The close energetic values suggest strong physisorption with partial charge transfer character rather than purely chemisorptive interaction. In both cases, however, configuration (1) is slightly more thermodynamically favorable, suggesting marginally stronger binding.

Geometric analysis reveals that lorazepam adsorbs parallel to the curved π-surface of C_{60} in both configurations as shown in Fig. 2, enabling maximum contact between the aromatic

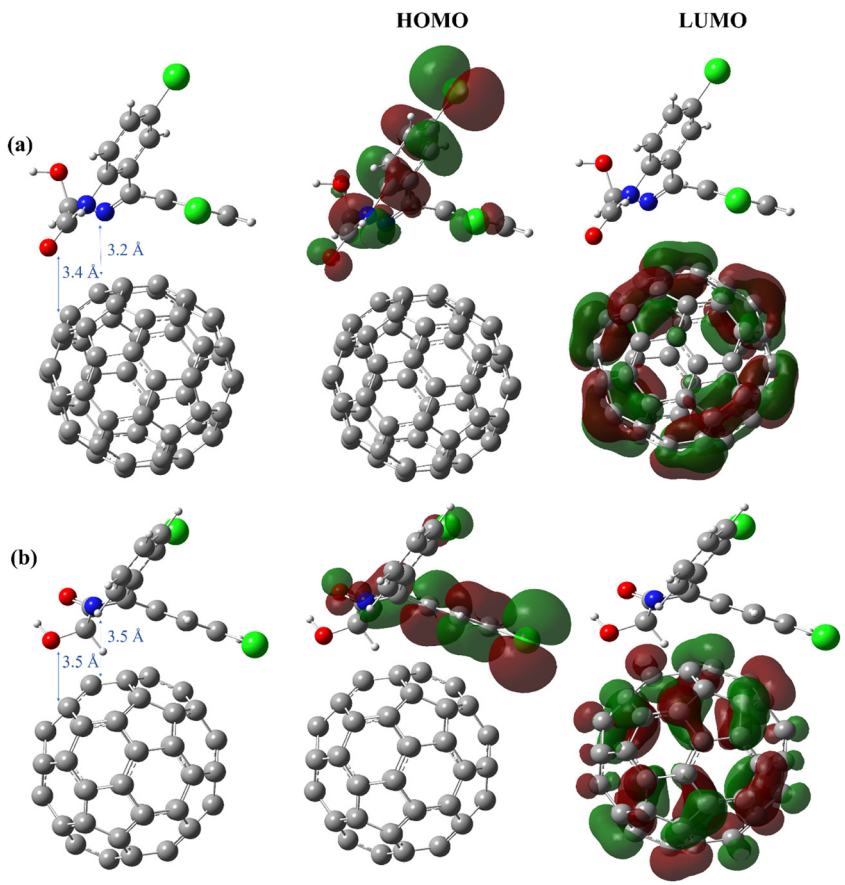

Fig. 2 The optimized models for most stable complexes: (a) configuration (1) and (b) configuration (5) of the lorazepam drug onto pristine C_{60}, respectively, and their HOMO and LUMO orbital.

rings of the drug and the fullerene surface. The equilibrium adsorption distances fall within the range of 3.2–3.4 Å for configuration (1) and 3.5 Å for configuration (5). Despite these moderate interaction distances, the large magnitude of the adsorption energies indicates enhanced interaction strength compared to typical physisorption systems. The shorter interaction distance observed in configuration (1) directly explains its slightly more negative adsorption energy, indicating a stronger drug–C_{60} interaction.

In addition to π–π interactions, the orientation of the heteroatoms plays a crucial role in stabilizing the complexes. The oxygen and nitrogen atoms of lorazepam are favorably oriented toward electron deficient regions of the C_{60} surface, promoting significant electronic interaction and charge redistribution. Moreover, the chlorine substituent contributes sterically to the adsorption stability. In configuration (1), the Cl atom is oriented away from the fullerene surface, minimizing steric repulsion and allowing closer approach of the aromatic framework, whereas in configuration (5), the slightly increased adsorption distance of 3.5 Å reflects reduced surface contact.

In Fig. 3e and f, the RDG-NCI analysis further supports the presence of strong interaction. Localized charge redistribution is observed at the adsorption interface, indicating polarization and partial charge transfer between lorazepam and the fullerene surface, consistent with chemisorption.

This interpretation is fully supported by frontier molecular orbital (FMO) analysis, as shown in Fig. 2. The HOMO is mainly localized on the lorazepam molecule, while the LUMO is predominantly distributed over the C_{60} surface, with noticeable spatial interaction between them. Such HOMO–LUMO interaction is consistent with chemisorption and suggests electronic coupling between the drug and the surface. The HOMO and LUMO for the remaining configurations (2, 3, and 4) under vacuum are illustrated in Fig. S1.

In Fig. 3c and d, partial density of states (PDOS) analysis provides additional insight into the electronic interaction strength. Configuration (1) exhibits a higher density of occupied states near the valence region and more pronounced virtual states close to the Fermi level compared to configuration (5). This enhanced electronic contribution correlates well with the shorter adsorption distance and more negative adsorption energy, reinforcing the superior stability of configuration (1), and supporting its partial chemisorption character.

Vibrational analysis confirms the structural stability of both complexes, as no imaginary frequencies are detected in their IR spectra, as shown in Fig. 3a and b. Notably, configuration (1) shows slightly stronger vibrational perturbations in the fingerprint region, reflecting stronger intermolecular interactions and a more constrained adsorption geometry, in agreement with its reduced equilibrium distance and enhanced electronic coupling. The corresponding analyses for the remaining configurations (2, 3, and 4) are provided in Fig. S2, including RDG, NCI, PDOS, and IR spectra, and their HOMO–LUMO are shown in Fig. S1.

Overall, the combined geometric, vibrational, and electronic analyses clearly demonstrate that configurations (1) and (5) represent the most stable adsorption modes of lorazepam on pristine C_{60}. The energetic magnitude, −4.70 eV and −4.67 eV, confirms strong physisorption with partial charge transfer. The relatively high adsorption energies indicate enhanced interaction strength compared to typical physisorption systems, while the marginal energetic advantage of configuration (1) arises from its shorter adsorption distance from 3.2 to 3.4 Å, optimal molecular orientation, and stronger electronic interaction with the fullerene surface. These results provide a clear

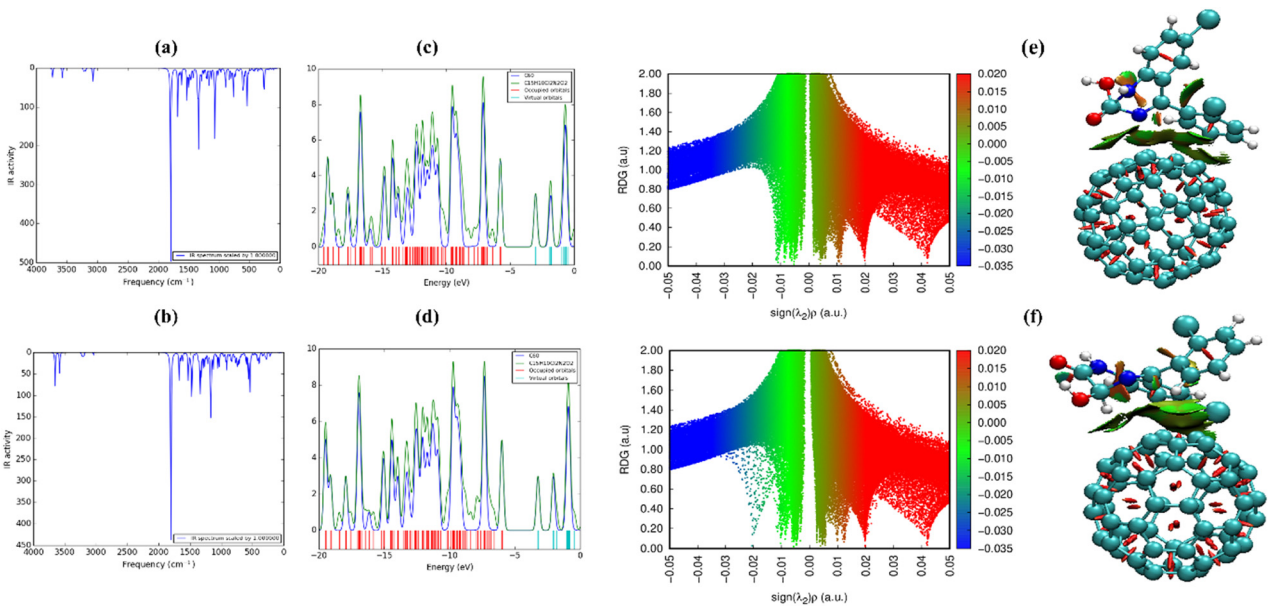

Fig. 3 The IR spectra (a) and (b), and partial density of states (PDOS) spectra (c) and (d). The RDG (left) and NCI (right) are shown in (e) and (f) under vacuum for the most stable configurations (1, 5) of lorazepam adsorbed on C_{60}, respectively.

molecular level understanding of lorazepam adsorption on C_{60} and establish a solid foundation for the subsequent investigation of heteroatom-doped fullerene systems aimed at further enhancing adsorption performance.

3.2. Modulated lorazepam adsorption over SiC_{59}

This study investigates the adsorption behavior of lorazepam on SiC_{59} through two distinct adsorption configurations, denoted as configuration (1) and configuration (5). The results clearly demonstrate that silicon doping plays a crucial role in creating an active adsorption site on the fullerene surface, significantly enhancing the interaction between the drug molecule and C_{60} compared to the pristine structure.

In Fig. 4a, lorazepam approaches the silicon atom at a short distance of approximately 1.8 Å, indicating a strong interaction characteristic of chemisorption. This structural proximity is reflected in a high adsorption energy of −6.1 eV under vacuum, confirming the formation of a highly stable complex suitable for drug loading applications, because of strong orbital overlap between the drug molecule and the SiC_{59} surface. In contrast, configuration (5), which is shown in Fig. 4b, exhibits a larger adsorption distance of about 4.2 Å, corresponding to a weaker chemisorptive interaction compared to configuration (1), with an adsorption energy of −4.7 eV under vacuum. Although less intense than configuration (1), this value still confirms chemisorption, highlighting the effectiveness of silicon doping in strengthening adsorption even at less favorable orientations.

HOMO–LUMO analysis (Fig. 4) reveals that silicon doping induces a significant redistribution of electron density within the system, indicating effective charge transfer between the two components.

Based on the short interaction distance of approximately 1.8 Å, the high adsorption energy of −6.1 eV, and the significant NBO stabilization energy of 92.28 kcal mol^{-1}, the interaction in SiC_{59} is classified as chemisorption. Four converging criteria define this classification: adsorption energies exceeding −3 eV, interaction distances below 2.5 Å, NBO stabilization energies exceeding 20 kcal mol^{-1}, and significant PDOS orbital overlap near the Fermi level.

3.3. Enhanced lorazepam adsorption on GeC_{59}

The optimized geometries, electronic structures, vibrational spectra, and partial density of states analyses further confirm the strong interaction between lorazepam and the GeC_{59} surface for both adsorption configurations (1) and (5). As shown in the optimized structures, lorazepam approaches the Ge active site with short interaction distances of about 2 Å for configuration (1) and 2.6 Å for configuration (5), indicating chemisorption behavior, although weaker than the Si-doped systems.

This is supported by the highly negative adsorption energies, where configuration (1) exhibits an adsorption energy of

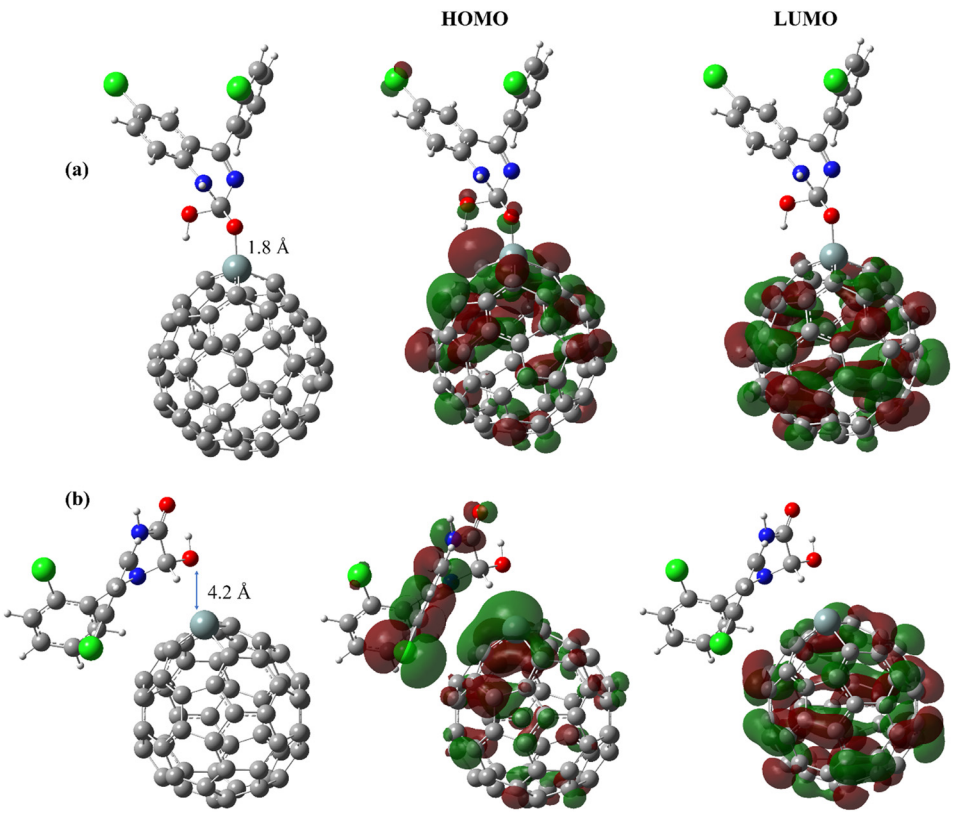

Fig. 4 The optimized models of the lorazepam drug adsorbed onto SiC_{59} for (a) configuration (1), and (b) configuration (5), respectively with their HOMO and LUMO orbitals.

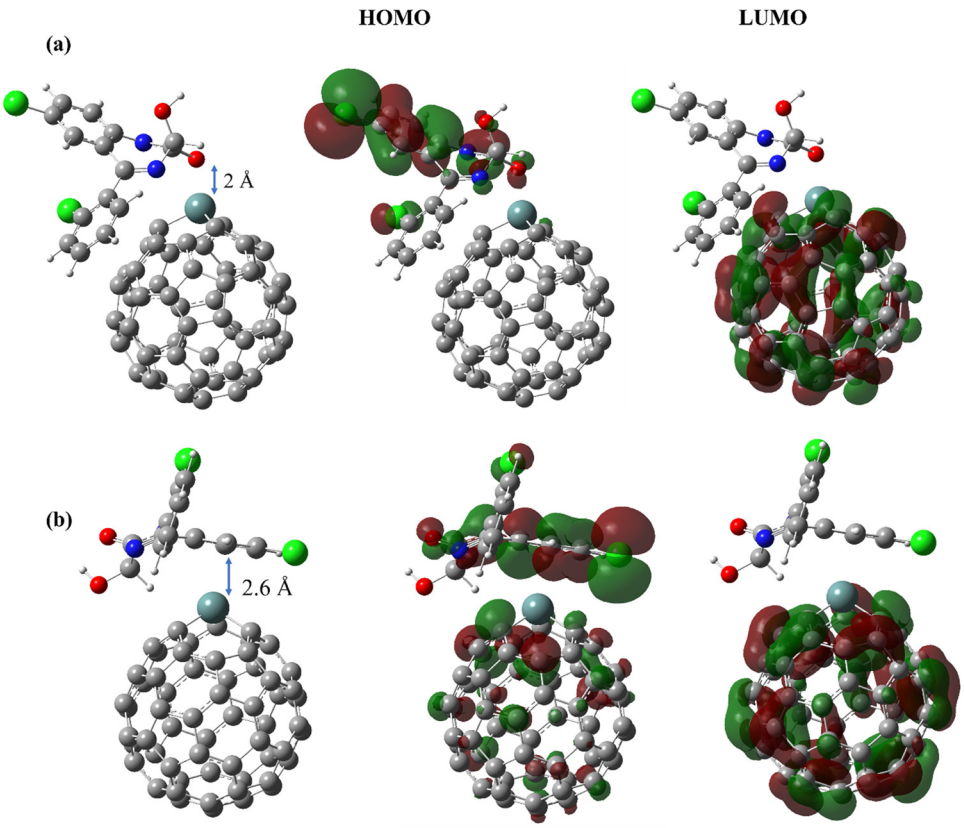

Fig. 5 The optimized models of the lorazepam drug adsorbed onto GeC_{59} (a) and (b) and their HOMO and LUMO with various orientations: (a) configuration (1), and (b) configuration (5).

−5.84 eV, while configuration (5) shows a slightly more negative value of −5.85 eV, confirming the energetic stability of both complexes with a marginal preference for configuration (5).

Fig. 5 illustrates the HOMO–LUMO distributions, revealing a pronounced redistribution of the frontier molecular orbitals upon adsorption. The HOMO is mainly localized on the lorazepam molecule with partial contribution from the Ge atom, whereas the LUMO is predominantly delocalized over the GeC_{59} nanocage. This orbital overlap facilitates charge transfer from the drug molecule toward the doped fullerene surface, enhancing the adsorption strength.

The adsorption behavior of lorazepam on doped fullerene surfaces is further clarified through vibrational and electronic structure analyses, as presented in Fig. 6. The IR spectra shown in Fig. 6(a) and (d) exhibit noticeable shifts in both the positions and intensities of several vibrational bands after adsorption, particularly those associated with the active functional groups of lorazepam. These changes indicate the direct involvement of these groups in the adsorption process and reflect the structural perturbations induced by interaction with the doped C_{60} surfaces.

The corresponding partial density of states (PDOS) spectra depicted in Fig. 6(e) and (h) reveal significant modifications in the electronic structure upon adsorption. An increased density of electronic states near the Fermi level, along with enhanced overlap between the molecular orbitals of lorazepam and the electronic states of the substrate, is observed for both the SiC_{59} and GeC_{59} systems. This behavior indicates enhanced electronic coupling and a reduction in the effective energy gap, suggesting improved electronic conductivity following adsorption.

A comparative analysis shows that the SiC_{59} system exhibits slightly stronger electronic interaction with lorazepam than the GeC_{59} counterpart, consistent with the more pronounced orbital overlap and higher stability observed for SiC_{59}. Nevertheless, both dopants significantly enhance the adsorption capability of pristine C_{60}. Similarly, for GeC_{59}, the short interaction distances of 2.0 to 2.6 Å and NBO stabilization energies of 22.5 kcal mol^{-1} confirm the chemisorption nature of the interaction, although it remains slightly weaker than that observed for the SiC_{59} system.

The relatively high adsorption energies observed for the doped systems can be attributed to strong donor–acceptor interactions between the heteroatom dopant and the functional groups of lorazepam. The presence of silicon or germanium introduces highly active adsorption sites on the fullerene surface and enhances charge transfer between the drug molecule and the nanocage, leading to stronger binding compared with pristine C_{60} and explaining the increased adsorption stability observed for the doped systems.

3.4. Exploring non-covalent interactions: insights from reduced density gradient analysis

To elucidate the adsorption mechanism, we performed non-covalent interaction (NCI) analysis and reduced density

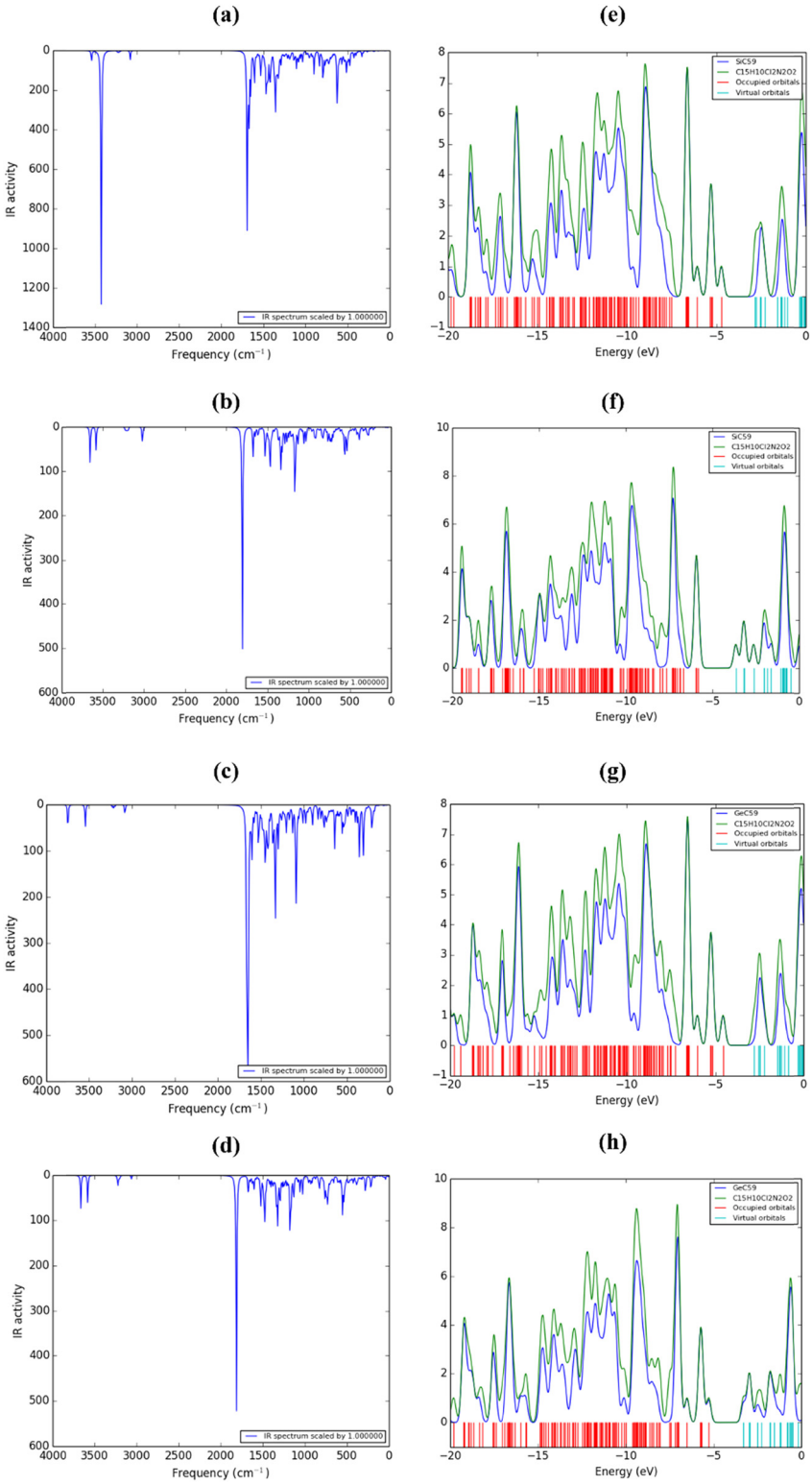

Fig. 6 The IR spectra (a)–(d), as well as the partial density of states (PDOS) spectra (e)–(h) of the lorazepam drug adsorbed onto SiC_{59} and GeC_{59} of two configurations (1 and 5), respectively.

gradient (RDG) mapping for the lorazepam drug adsorbed on pristine C_{60}, SiC_{59}, and GeC_{59} under vacuum conditions. These visual tools clearly differentiate weak interactions – including hydrogen bonding, van der Waals forces (vdW), and steric repulsions – providing critical insights into the stability and nature of the drug–surface interactions.[71,73] The RDG is derived

from the electron density (ρ) and its gradient, as defined by eqn (5):

$$\mathrm{RDG} = \frac{1}{2(3\pi^2)^{1/3}} \frac{|\nabla\rho|}{\rho^{4/3}} \quad (5)$$

Analysis of RDG *versus* sign(λ_2)ρ plots enables identification of interaction types:

Negative sign(λ_2)ρ values (green-blue regions) correspond to attractive forces (*e.g.*, hydrogen bonding, π–π interactions). Positive values (red regions) indicate steric repulsion and when ρ approaches zero, the interactions are characteristic of van der Waals forces.

In (Fig. 7a and b), the RDG *versus* sign(λ_2)ρ plots and corresponding NCI iso-surfaces for the SiC_{59}–lorazepam configurations are presented. The RDG plots show pronounced spikes in the negative sign(λ_2)ρ region, indicating the presence of significant attractive interactions, associated with strong adsorption. These interactions are further confirmed by the green and blue regions in the NCI iso-surfaces, which are localized around the Si dopant and the nearby functional groups of lorazepam. This behavior suggests that Si doping creates an effective active site, enhancing charge redistribution and strengthening adsorption through electrostatic and donor–acceptor interactions and partial covalent character.

In contrast, Fig. 7c and d illustrate the GeC_{59}–lorazepam complexes. Although attractive interactions are still observed, the intensity of the negative sign(λ_2)ρ spikes is relatively weaker compared to the Si-doped case. The NCI iso-surfaces are dominated by green regions with fewer blue areas, indicating comparatively weaker attractive interactions than in the Si system, yet still consistent with chemisorption. This implies that Ge doping is less effective than Si doping in activating the fullerene surface toward strong adsorption.

Overall, the comparison demonstrates that SiC_{59} exhibits stronger and more localized attractive interactions than GeC_{59}, which explains the higher adsorption stability observed for the Si-doped configurations.

3.5. Global indices parameters

We calculated global reactivity descriptors, including electron affinity (E_A), ionization potential (IP), electrophilicity index (ω), chemical potential (μ_{ch}), chemical hardness (η), and softness (χ) to assess the electronic reactivity and stability of the system. These global indices provide essential insights into the nature of molecular interactions and reactivity of the lorazepam drug on the C_{60} surface. Their respective expressions are given below:[68,74]

Electron affinity (E_A), which indicates a molecule's ability to accept electrons (LUMO energy):

$$E_A = -E_L \quad (6)$$

The ionization potential (IP), which provides a molecule's ability to donate electrons (HOMO energy):

$$\mathrm{IP} = -E_H \quad (7)$$

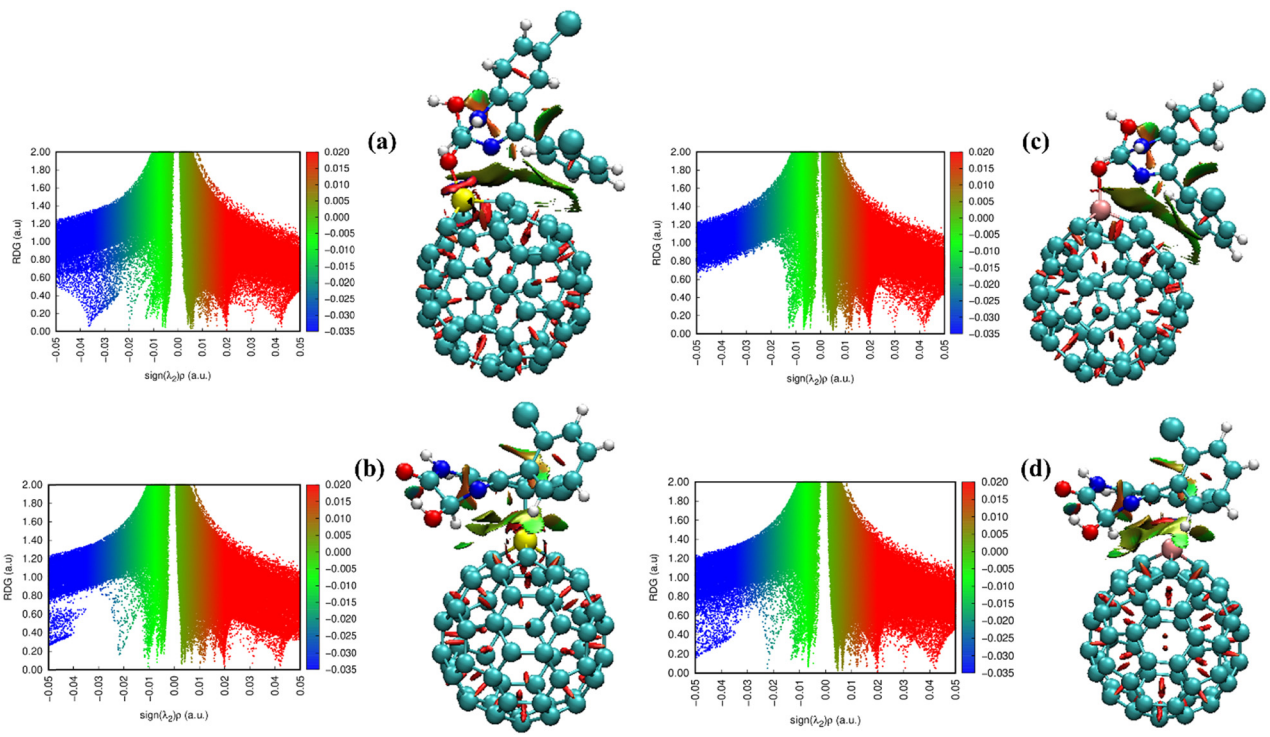

Fig. 7 RDG (left) and NCI (right) analyses under vacuum for lorazepam adsorption on (a) and (b) SiC_{59} and (c) and (d) GeC_{59} surfaces for configurations (1) and (5).

The electrophilicity index (ω), which reflects the molecule's tendency to accept electrons to form bonds with nucleophilic molecules:

$$\omega = \frac{\mu^2}{2\eta} \tag{8}$$

Additionally, the HOMO and LUMO orbitals, along with the molecular electrostatic potential (MESP), are sometimes used to enhance the prediction of the adsorption mechanism.[75–80]

Chemical potential (μ_{ch}):

$$\mu_{ch} = \frac{-(IP + EA)}{2} \tag{9}$$

Chemical hardness (η):

$$\eta = \frac{(IP - EA)}{2} \tag{10}$$

Softness (χ):

$$\chi = \frac{1}{\eta} \tag{11}$$

3.6. Work function

The adsorption of lorazepam affects the work function (φ) of the nanocarrier, reflecting changes in electronic properties. The work function is defined as:[72]

$$\varphi = V_\infty - E_F \tag{12}$$

where V_∞ and E_F are electrostatic potential energy far from the material surface and Fermi energy, respectively. From the above equation, if $V_\infty = 0$, this implies $\varphi = -E_F$. The variation in φ upon adsorption indicates redistribution of electronic density, confirming strong interaction between lorazepam and the nanocarrier surface.

These descriptors, especially under vacuum (as shown in Table 1), are widely used to predict molecular reactivity, and complement experimental adsorption studies.[75,81–86] The stability of molecular orientations plays a crucial role in adsorption behavior, as certain configurations may exhibit stability in the doped state but lack it in the non-doped state. This difference in stability significantly influences adsorption energy, leading to remarkable differences in adsorption performance. Although the interactions are strong and stable under vacuum, the adsorption remains stable and energetically favorable in aqueous environments.

3.7. Thermodynamic analysis

The thermodynamic parameters of the optimized complexes were determined through harmonic frequency analysis under standard conditions (298.15 K, 1 atm). Gibbs free energy (ΔG), enthalpy (ΔH) and entropy (ΔS) values for all five orientationally distinct complexes under vacuum and in a solvent are summarized in Table 2. The relative stability of the inclusion complexes was assessed by comparing the Gibbs free energy of each complex to the combined Gibbs free energies of its adsorbent and adsorbate. Negative ΔG values confirm spontaneous complex formation at 25 °C, and to drive spontaneous complexation and improve efficiency, strategic doping (*e.g.*, with Si or Ge) is proposed.

The negative values of both enthalpy (ΔH) and entropy (ΔS) suggest an enthalpy-driven inclusion process. Meanwhile, the negative ΔS reflects restricted mobility of the encapsulated guest molecule due to the constrained cavity of the host framework.

$$\Delta G = G_{com} - (G_{host} + G_{guest}) \tag{13}$$

$$\Delta H = H_{com} - (H_{host} + H_{guest}) \tag{14}$$

$$\Delta S = S_{com} - (S_{host} + S_{guest}) \tag{15}$$

3.8. Solvent effect

To assess the adsorption behavior of pristine C_{60}, SiC_{59}, and GeC_{59} in an aqueous environment, the binding energies (E_{bind}) of the lorazepam–surface complexes were systematically investigated in water. All geometries of the lorazepam–C_{60}, lorazepam–SiC_{59}, and lorazepam–GeC_{59} complexes were fully re-optimized using the IEFPCM implicit solvation model

Table 1 HOMO and LUMO energies (E_{HOMO} and E_{LUMO}), HOMO–LUMO gap (E_G), difference in E_g (ΔE_g), ionization potential (IP), electron affinity (EA), chemical hardness (η), softness (χ), chemical potential (μ_{ch}), electrophilicity index (ω), Fermi level (E_F), binding energies (E_{bind}), and work function for systems of lorazepam–C_{59}, lorazepam–SiC_{59}, and lorazepam–GeC_{59} with different orientations under vacuum

System	HOMO (eV)	LUMO (eV)	E_G (eV)	ΔE_g (eV)	IP (eV)	E_A (eV)	η (eV)	χ $(eV)^{-1}$	μ_{ch} (eV)	ω (eV)	E_F (eV)	E_{bind} (eV)	Work function (φ)
Config. 1	−5.75	−3.02	−2.731	−0.03	5.75	3.02	1.37	0.73	−4.38	7.03	−4.38	−4.70	4.38
Config. 2	−5.98	−3.24	−2.73	−0.03	5.98	3.24	1.37	0.73	−4.61	7.78	−4.61	−4.66	4.61
Config. 3	−5.89	−3.16	−2.73	−2.73	5.89	3.16	1.37	0.73	−4.53	7.51	−4.53	−4.63	4.53
Config. 4	−5.89	−3.16	−2.74	−0.03	5.89	3.16	1.37	0.73	−4.53	7.48	−4.53	−4.62	4.53
Config. 5	−5.98	−3.24	−2.74	−0.03	5.98	3.24	1.37	0.73	−4.61	7.76	−4.61	−4.67	4.61
SiC_{59}													
Config. 1	−4.72	−2.85	−1.88	−0.29	4.72	2.85	0.94	1.07	−3.78	7.63	−3.78	−6.08	3.78
Config. 5	−5.83	−3.66	−2.17	0.002	5.83	3.66	1.09	0.92	−4.74	10.36	−4.74	−4.71	4.74
GeC_{59}													
Config. 1	−4.56	−2.81	−1.76	−0.36	4.56	2.81	0.88	1.14	−3.68	7.72	−3.68	−5.84	3.68
Config. 5	−5.28	−3.30	−1.98	−0.14	5.28	3.30	0.99	1.01	−4.29	9.31	−4.29	−5.85	4.29

Table 2 The calculated thermodynamic parameters, enthalpy (ΔH), Gibbs free energy (ΔG), and entropy (ΔS), of the studied complexes lorazepam–C_{60}, lorazepam–SiC_{59}, and lorazepam–GeC_{59} with different orientations under vacuum and in a solvent

System	ΔH (eV)	ΔG (eV)	ΔS (eV)
Vacuum			
C_{60}			
Config. 1	−4.62	−4.16	−0.0015
Config. 2	−4.58	−4.11	−0.0016
Config. 3	−4.55	−4.07	−0.0016
Config. 4	−4.55	−4.05	−0.0016
Config. 5	−4.59	−4.10	−0.0016
SiC_{59}			
Config. 1	−5.96	−5.47	−0.0016
Config. 5	−4.64	−4.16	−0.0016
GeC_{59}			
Config. 1	−5.76	−5.17	−0.0019
Config. 5	−5.31	−4.80	−0.0017
Solvent			
C_{60}			
Config. 1	−4.52	−4.04	−0.0016
Config. 2	−4.55	−4.07	−0.0016
Config. 3	−4.52	−4.03	−0.0016
Config. 4	−4.51	−4.03	−0.0016
Config. 5	−4.55	−4.07	−0.0016
SiC_{59}			
Config. 1	−6.12	−5.53	−0.0019
Config. 5	−4.88	−4.33	−0.0018
GeC_{59}			
Config. 1	−5.98	−5.38	−0.00197
Config. 5	−5.48	−4.88	−0.00196

combined with the hybrid B3LYP functional and the 6-31G(d) basis set, including empirical dispersion corrections (B3LYP-D3, Grimme's GD3) to accurately account for long-range van der Waals interactions. The inclusion of solvent and dispersion effects resulted in noticeable modifications to the optimized geometrical parameters, reflecting solvent-induced rearrangements that enhance intermolecular interactions at the drug–surface interface. In addition, global reactivity indices were calculated in the solvent phase (Table S1) to provide further insight into the electronic properties of the investigated systems. Importantly, the Gibbs free energy of adsorption (ΔG) in water, reported in Table 2, provides a more realistic measure of stability under physiological conditions than electronic adsorption energies alone. The negative ΔG values ranging from −4.04 to −5.53 eV confirm that complex formation remains spontaneous and stable in aqueous environments, with SiC_{59} showing the highest stability at −5.53 eV for configuration (1).

For pristine C_{60}, the aqueous environment alters the relative stability of the adsorption configurations, rendering configuration (5) the most favorable with an adsorption energy of −4.64 eV. Although solvation slightly weakens the adsorption strength compared to the vacuum phase, the interaction remains sufficiently strong, indicating that lorazepam adsorption on pristine C_{60} is stable under realistic solvent conditions.

In the case of SiC_{59}, solvation exerts a more pronounced effect on both geometry and energetics. Configuration (1) becomes the most thermodynamically stable structure in water, exhibiting a significantly enhanced adsorption energy of −6.23 eV. This improvement highlights the crucial role of solvent polarization and dispersion interactions in improving the adsorption efficiency of the Si-doped system by stabilizing favorable adsorption orientations and strengthening dipole–dipole and charge-transfer interactions. The synergistic effect of silicon doping, solvent effects, and dispersion contributions leads to superior interaction efficiency compared to pristine C_{60} and the corresponding vacuum-phase results.

Similarly, for GeC_{59}, configuration (1) emerges as the most stable adsorption mode in the aqueous environment, with an adsorption energy of −6.07 eV. This stabilization can be attributed to improved dipolar alignment, and favorable electrostatic contributions between lorazepam and the Ge-doped surface, accompanied by subtle solvent-induced geometric rearrangements.

The solvation energy (E_{sol}) values listed in Table S1 are negative for all studied systems, indicating that solvation is a thermodynamically favorable process and enhances the stability of the complexes in the solvent. Among all systems, for lorazepam–GeC_{59}, configuration (1) exhibits the most negative solvation energy, making it the most stable system and suggesting the strongest interaction with the solvent.

Overall, while the general stability trends observed under vacuum are largely preserved, solvation in water induces noticeable changes in both geometry and thermodynamic preference among the adsorption configurations. Importantly, the solvent and dispersion effects do not drastically diminish the overall adsorption strength; instead, they enhance the adsorption efficiency, particularly in the SiC_{59} system, by promoting more favorable interaction mechanisms. The optimized configurations and analysis in aqueous environments (Fig. S3–S7) for pristine C_{60}, SiC_{59}, and GeC_{59} further confirm that water primarily modulates the relative energetic ordering of the adsorption modes while maintaining strong and stable drug–surface interactions across different environments.

3.9. The natural bond orbital (NBO) charge analysis

Natural bond orbital (NBO) analysis was carried out to gain deeper insight into the nature of intermolecular interactions and charge-transfer mechanisms between the lorazepam molecule and pristine as well as doped C_{60} surfaces. The interaction parameters, including the second-order perturbation stabilization energy ($E^{(2)}$), the energy difference between donor and acceptor orbitals ($E_{(j)} - E_{(i)}$), and the Fock matrix element ($F_{(i,j)}$), were analyzed to evaluate the strength and character of donor–acceptor interactions. The second-order stabilization energy ($E^{(2)}$), estimated from the Fock matrix, quantifies the delocalization energy associated with donor (i) to acceptor (j) orbital interactions and is calculated using the following expression:

$$E^{(2)} = q_i \frac{F_{(i,j)}^2}{E_j - E_i} \quad (16)$$

In the above equation, q_i presents the occupancy of the donor orbital, $E_{(j)}$ and $E_{(i)}$ are the diagonal elements

Table 3 The results of the donor and acceptor NBOs, as well as the second-order perturbation stabilization energies ($E^{(2)}$, kcal mol^{-1}), corresponding to the charge transfer of C_{60}, SiC_{59}, and GeC_{59} with lorazepam drug molecules under vacuum

System	Donor NBO (i)	Acceptor NBO (j)	$E^{(2)}$ (kcal mol^{-1})	$E_{(j)} - E_{(i)}$ (a.u.)	$F_{(i,j)}$ (a.u.)
Config. 1	LP (1) N 88	BD* (2) C 27–C 36	0.50	0.40	0.013
Config. 2	LP (1) O 86	BD* (2) C 13–C 14	0.10	0.61	0.008
Config. 3	LP (1) O 86	BD* (2) C 53–C 56	0.07	0.61	0.007
Config. 4	BD (2) C 29–C 37	BD* (2) C 67–C 68	0.26	0.27	0.008
Config. 5	BD (2) C 62–N 88	BD* (2) C 47–C 48	0.44	0.36	0.012
SiC_{59}					
Config. 1	LP (2) O 84	LP* (1) Si 91	92.89	0.65	0.226
Config.5	BD (2) C 47–Si 90	BD* (1) C 62–H 91	0.37	0.66	0.016
GeC_{59}					
Config. 1	LP (2) O 84	BD* (1) O 84–Ge 91	22.51	0.71	0.119
Config. 5	BD (2) C 66–C 67	LP* (1) Ge 90	13.99	0.33	0.064

corresponding to the acceptor and donor orbitals, respectively, and $F_{(i,j)}$ denotes the off-diagonal NBO Fock matrix element. The second-order perturbation stabilization energy ($E^{(2)}$) is directly proportional to the intensity of the donor–acceptor interaction. A stronger donor–acceptor interaction leads to a larger $E^{(2)}$ value, thereby increasing the overall stability of the C_{60}–drug complexes. For the pristine C_{60} system, the obtained $E^{(2)}$ values are relatively small, ranging from 0.07 to 0.93 kcal mol^{-1}. These weak stabilization energies mainly originate from $\pi \rightarrow \pi^*$ and $n \rightarrow \pi^*$ interactions between the lorazepam molecule and the fullerene surface, indicating limited charge transfer. Such low $E^{(2)}$ values suggest that the adsorption process on pristine C_{60} involves comparatively weaker donor–acceptor interactions relative to the doped systems, yet still consistent with partial chemisorption, as supported by the calculated adsorption energy. In contrast, a remarkable enhancement in donor–acceptor interactions is observed upon silicon doping. In the SiC_{59} system, an exceptionally strong interaction is detected for the LP (2) O $\rightarrow$ LP* (1) Si transition, with a stabilization energy of 92.89 kcal mol^{-1} and a high $F_{(i,j)}$ value of 0.226 a.u. This strong interaction indicates significant charge transfer from the lone pair of the oxygen atom in lorazepam to the vacant orbitals of the silicon dopant, reflecting the formation of a partially covalent bond. The presence of silicon introduces an electron-deficient active site on the C_{60} surface, thereby dramatically enhancing the adsorption strength and promoting chemisorption behavior.

Similarly, the GeC_{59} system exhibits stronger donor–acceptor interactions compared to the pristine system, although weaker than those observed for the silicon-doped structure. The LP (2) O $\rightarrow$ BD* (1) O–Ge interaction shows a stabilization energy of 22.51 kcal mol^{-1}, while the BD (2) C–C $\rightarrow$ LP* (1) Ge transition contributes 13.99 kcal mol^{-1}. These values confirm effective charge transfer between lorazepam and the Ge-doped surface, suggesting a moderate chemisorption interaction. The relatively lower E^2 values compared to SiC_{59} can be attributed to the reduced electron-accepting ability of germanium relative to silicon.

Overall, the NBO results clearly demonstrate that heteroatom doping significantly enhances charge transfer and intermolecular interactions, thereby improving the adsorption stability of lorazepam on the C_{60} surface. The strength of donor–acceptor interactions follows the order $SiC_{59} > GeC_{59} > C_{60}$, which is in excellent agreement with the calculated adsorption energies and electronic structure analyses. These findings support the potential application of doped C_{60} systems as efficient nanocarriers for lorazepam delivery. These parameters for each model of the complexes are summarized in Table 3.

4. Protonation-driven drug release under acidic conditions

The relatively high adsorption energies obtained for the doped systems indicate strong drug–carrier interactions, which are advantageous for drug loading. Despite this strong binding, these interactions can be significantly weakened under realistic environmental conditions, such as solvent effects, pH or temperature, enabling controlled drug release.

To investigate the possibility of lorazepam drug release behavior from the nanocarrier, a dual protonation model was applied to simulate the impact of acidic tumor microenvironment (pH < 7). Among the investigated systems, Config.1 of SiC_{59} was selected for the release invistigation due to its highest adsorption stability compared with the other studied configurations. Protonation was introduced at two key interaction sites: the ketone oxygen atom of the drug molecule and the dopant atom of the fullerene surface. The optimized structure shows a noticeable geometrical change upon protonation, where the equilibrium distance between the drug and the nanocarrier increases from 1.8 Å in the neutral system to 4.98 Å in the protonated system. This increase suggests considerable weakening in the interaction between the two components compared to the neutral state.

These results are supported by previous theoretical studies on similar nanocarrier systems, where protonation was shown to significantly reduce adsorption energy and promote drug desorption from carbon-based nanostructures.[87] In doped fullerene systems, protonation has been reported to induce strong weakening of drug–surface interactions, leading to partial or nearly complete separation of the drug molecule from the

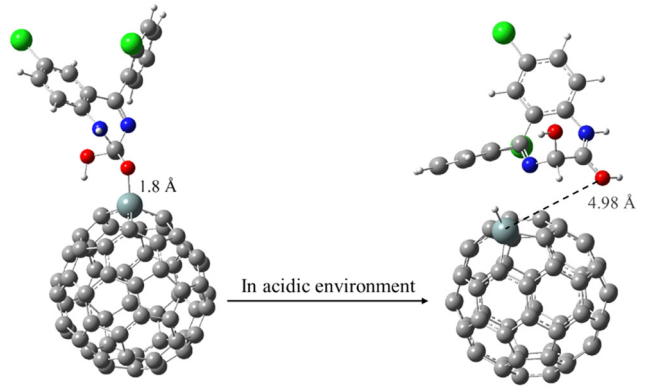

Fig. 8 The optimized structures for the bound drug–$C_{56}Si$ and the released drug where the coordination bond has been fully cleaved.

carrier.[88] Furthermore, studies on nitrogen-containing carbon frameworks demonstrated that acidic conditions lead to a substantial decrease in adsorption strength, indicating enhanced release behavior.[89] Other investigations revealed that protonation shifts the interaction regime from strong adsorption to weaker noncovalent interactions accompanied by an increase in drug–surface distance.[90] Additionally, it has been shown that protonation under acidic environments results in both reduced adsorption energy and increased separation distance, confirming a general trend of facilitated drug release[91] (Fig. 8).

Overall, the obtained results demonstrate that protonation under acidic conditions, known for the tumor microenvironment, weakens the interaction between the drug and the nanocarrier, supporting a pH-responsive release mechanism within the framework of density functional theory calculations.

5. Comparison of adsorption energy (E_{bind}) and adsorption distance (d) of the lorazepam drug adsorbed on pristine C_{60}, SiC_{59} and GeC_{59} with previously reported materials

The results of the present study clearly demonstrate stronger adsorption interactions, as reflected by the more negative binding energy values, particularly for the Si and Ge systems reaching −6.08 eV and −5.85 eV, respectively. These values are consistent with recent reports on high-performance drug delivery systems, including nitride-derived fullerenes with an adsorption energy of −6.521 eV for felodipine delivery, Stone–Wales defective graphene nanoribbons showing −6.027 eV for fluorouracil, and Nb_2C MXene quantum dots exhibiting −6.775 eV for fluorouracil adsorption. While earlier studies report weak to moderate adsorption on pristine and other modified fullerene structures, the doped systems investigated here exhibit significantly enhanced binding energies reaching approximately −6 eV, indicating a substantial enhancement in chemisorption strength. In addition, the shorter adsorption distances calculated in this work of 1.8 to 2.0 Å for the doped systems compared to most literature values further support the formation of stronger interfacial interactions.

Overall, this comparison highlights that silicon and germanium doping provides a more effective strategy for improving the adsorption performance of C_{60} than other previously reported modifications, and that the binding energies obtained are within the range reported for other promising drug delivery platforms, emphasizing the superior stability and adsorption capability of the systems studied in this work (Table 4). It should also be noted that the calculated adsorption energies are relatively high, reflecting very strong interactions between the drug and the nanocarrier surface. Although these values are obtained under the present computational conditions, effective interactions may be reduced under different environmental conditions, such as solvent effects, pH or temperature, thereby

Table 4 Comparison of binding energies (E_{bind} (eV)) and adsorption distances (d, Å) for the studied C_{60}, SiC_{59}, and GeC_{59} systems in different configurations, along with previously reported values from the literature

System	E_{bind} (eV)	d (Å)	Ref.
C_{60}			
Config. 1	−4.70	3.4	This work
Config. 5	−4.67	3.5	This work
SiC_{59}			
Config. 1	−6.08	1.8	This work
Config. 5	−4.71	4.2	This work
GeC_{59}			
Config. 1	−5.84	2	This work
Config. 5	−5.85	2.6	This work
AS			
C_{60}	−0.29	3.01	92
BC_{59}	−1.04	1.58	92
NC_{59}	−0.41	3.11	92
BNC_{58}	−0.96	1.57	92
MAT			
C_{60}	1.474	—	93
GaC_{59}	−1.263	—	93
AP			
C_{20} (II-isomer)	-5.61×10^4	1.620	94
Met			
C_{59}Si–C	−1.65	1.934	95
C_{59}Si–N	−0.90	1.850	95
C_{60}–C	0.055	1.580	95
MF			
C_{60}	0.0187	4.27	96
SiC_{59}	−1.61	1.79	96
PEG/C_{60}			
H	−0.95	—	97
G	−0.83	—	97
Nb_2C-s-Flu	−6.775	2.053	98
Nb_2C-e-Flu	−3.576	2.132	98
GaNF	−6.521	—	99
FU/AGNRs-SW	−6.027	—	100
TP/AGNRs-SW	−5.917	—	100
HU/AGNRs-SW	−7.534	—	100
NU/AGNRs-SW	−8.972	—	100

allowing reversible binding or drug release. In fact, the tumor microenvironment is known to be acidic, which can lead to protonation of the chemical system and facilitate drug release, as reported in previous studies.[87–91]

6. Conclusion

A density functional theory (DFT) study was carried out to evaluate pristine and doped C_{60} nanocages as potential drug carriers for lorazepam. The results show that pristine C_{60} exhibits relatively weak adsorption compared with the doped systems. Doping with silicon or germanium significantly enhances the interaction strength by creating active adsorption sites and promoting charge transfer between the drug molecule and the fullerene surface. Among the studied systems, SiC_{59} demonstrates the strongest adsorption with an adsorption energy of approximately −6.1 eV and shorter interaction distances, indicating the formation of a highly stable drug–carrier complex. GeC_{59} also improves the adsorption behavior compared with pristine C_{60}, although its interaction remains weaker than that of SiC_{59}.

Electronic structure analyses, including HOMO–LUMO, PDOS, and NBO charge transfer confirm strong electronic interactions between lorazepam and the doped nanocages. Thermodynamic calculations further indicate that the adsorption process is energetically favorable and remains stable under aqueous conditions. Overall, the results suggest that doped C_{60} nanocages, especially SiC_{59}, are promising candidates for lorazepam delivery. Additionally, protonation under acidic conditions reduces the adsorption strength, suggesting a feasible pH-responsive drug release mechanism.

Author contributions

Mariam M. Seliem: computational analysis, investigation, data curation, visualization, formal analysis, methodology, writing – original draft. Mohamed M. Aboelnga: supervision, validation, conceptualization, project administration, computational analysis, investigation, visualization, data analysis, software, resources, writing – review & editing. Elsayed El-bayoumy: supervision, validation, conceptualization, writing – review & editing, Mohsen El-Tahawy: supervision, validation, conceptualization, computational analysis, investigation, visualization, data analysis, software, resources, writing – review & editing.

Conflicts of interest

The authors declare that they have no known competing financial interests or personal relationships that could have appeared to influence the work reported in this paper.

Data availability

Supplementary information (SI) is available. See DOI: https://doi.org/10.1039/d6ma00154h.

Acknowledgements

This research did not receive any specific grant from funding agencies in the public, commercial, or not-for-profit sectors.

References

1 A. R. Hashmi, M. Sekar, F. Zahra, N. Molugulu and L. S. Wong, Advanced drug delivery strategies to overcome solubility and permeability challenges: Driving biopharmaceutical advancements toward commercial success, *ACS Omega*, 2025, **10**(36), 40769–40792.
2 T. M. Allen and P. R. Cullis, Drug delivery systems: entering the mainstream, *Science*, 2004, **303**(5665), 1818–1822.
3 A. Tariq, S. Nazir, A. W. Arshad, F. Nawaz, K. Ayub and J. Iqbal, DFT study of the therapeutic potential of phosphorene as a new drug-delivery system to treat cancer, *RSC Adv.*, 2019, **9**(42), 24325–24332, DOI: 10.1039/c9ra02778e.
4 T. C. Ezike, U. S. Okpala, U. L. Onoja, C. P. Nwike, E. C. Ezeako and O. J. Okpara, *et al.*, Advances in drug delivery systems, challenges and future directions, *Heliyon*, 2023, **9**(6), e17488.
5 J. Florek, R. Caillard and F. Kleitz, Evaluation of mesoporous silica nanoparticles for oral drug delivery-current status and perspective of MSNs drug carriers, *Nanoscale*, 2017, **9**(40), 15252–15277, DOI: 10.1039/c7nr05762h PubMed PMID: 28984885.
6 P. Bhattarai, S. Hameed and Z. Dai, Recent advances in anti-angiogenic nanomedicines for cancer therapy, *Nanoscale*, 2018, **10**, 5393–5423, DOI: 10.1039/c7nr09612g PubMed PMID: 29528075.
7 E. G. C. Clarke, Analysis of Drugs and Poisons, *Pharmaceuticals, Body Fluids and Postmortem Material. Pharmaceutical*, 2004.
8 H. A. Archontaki, K. Atamian, I. E. Panderi and E. E. Gikas, Kinetic study on the acidic hydrolysis of lorazepam by a zero-crossing first-order derivative UV-spectrophotometric technique, *Talanta*, 1999, **48**(3), 685–693.
9 A. A. Kyriakopoulos, D. J. Greenblatt and R. I. Shader, Clinical pharmacokinetics of lorazepam: a review, *J. Clin. Psychiatry*, 1978, **39**(10 Pt 2), 16–23.
10 H. W. Elliott, Metabolism of lorazepam, *Br. J. Anaesth.*, 1976, **48**(10), 1017–1023.
11 G. C. Preston, P. Broks, M. Traub, C. Ward, P. Poppleton and S. M. Stahl, Effects of lorazepam on memory, attention and sedation in man, *Psychopharmacology*, 1988, **95**(2), 208–215.
12 Y. Zhang, T. R. Nayak, H. Hong and W. Cai, Graphene: a versatile nanoplatform for biomedical applications, *Nanoscale*, 2012, **4**(13), 3833–3842.
13 O. C. Farokhzad and R. Langer, Impact of nanotechnology on drug delivery, *ACS Nano*, 2009, **3**(1), 16–20.
14 N. Nasongkla, E. Bey, J. Ren, H. Ai, C. Khemtong and J. S. Guthi, *et al.*, Multifunctional polymeric micelles as cancer-targeted, MRI-ultrasensitive drug delivery systems, *Nano Lett.*, 2006, **6**(11), 2427–2430.

15 S. Haghgoo and A. Nekoei, Metal oxide adsorption on fullerene C60and its potential for adsorption of pollutant gases; density functional theory studies, *RSC Adv.*, 2021, **11**(28), 17377–17390, DOI: 10.1039/d1ra02251b.
16 Z. Liao, G. Song, Z. Yang and H. Ren, Adsorption and desorption behaviors of hydroxyurea drug on delivery systems of B12N12 fullerene and its Al-, Si-and P-dopings from theoretical perspective, *Mol. Phys.*, 2021, **119**(11), e1921296.
17 A. Montellano, T. Da Ros, A. Bianco and M. Prato, Fullerene C 60 as a multifunctional system for drug and gene delivery, *Nanoscale*, 2011, **3**(10), 4035–4041.
18 M. T. Aziz, W. A. Gill, M. K. Khosa, S. Jamil and M. R. S. A. Janjua, Adsorption of molecular hydrogen (H2) on a fullerene (C60) surface: insights from density functional theory and molecular dynamics simulation, *RSC Adv.*, 2024, **14**(49), 36546–36556, DOI: 10.1039/d4ra06171c.
19 S. Haghgoo and A. Nekoei, Metal oxide adsorption on fullerene C60and its potential for adsorption of pollutant gases; density functional theory studies, *RSC Adv.*, 2021, **11**(28), 17377–17390, DOI: 10.1039/d1ra02251b.
20 M. Bilge, Adsorption mechanism and structural investigation of doped C60 fullerenes with pentylamine, *Anadolu Univ. J. Sci. Technol. – Appl. Sci. Eng.*, 2017, **18**, 398–402, DOI: 10.18038/aubtda.281646.
21 K. R. S. Chandrakumar and S. K. Ghosh, Alkali-metal-induced enhancement of hydrogen adsorption in C60 fullerene: an ab initio study, *Nano Lett.*, 2008, **8**(1), 13–19.
22 S. W. de Silva, A. Du, W. Senadeera and Y. Gu, Neutral and charged boron-doped fullerenes for CO2 adsorption, *Beilstein J. Nanotechnol.*, 2014, **5**(1), 413–418, DOI: 10.3762/bjnano.5.49.
23 M. Cummings, S. Gliga, B. Lukanov, E. I. Altman, M. Bode and E. V. Barrera, Surface interactions of molecular C60 and impact on Ni (100) and Co (0001) film growth: A scanning tunneling microscopy study, *Surf. Sci.*, 2011, **605**(1–2), 72–80.
24 A. S. Rad, S. M. Aghaei, E. Aali, M. Peyravi and M. Jahanshahi, Application of chromium-doped fullerene as a carrier for thymine and uracil nucleotides: Comprehensive density functional theory calculations, *Appl. Organomet. Chem.*, 2018, **32**(2), e4070.
25 Q. Z. Li, J. J. Zheng, J. S. Dang and X. Zhao, Boosting activation of oxygen molecules on C60 fullerene by boron doping, *ChemPhysChem*, 2015, **16**(2), 390–395, DOI: 10.1002/cphc.201402620.
26 C. Parlak, Ö. Alver and M. Şenyel, Computational study on favipiravir adsorption onto undoped-and silicon-decorated C60 fullerenes, *J. Theor. Comput. Chem.*, 2017, **16**(02), 1750011.
27 P. Guo, H. Zhang, S. Dong and L. An, Density functional theory study of B-and Si-doped carbons and their adsorption interactions with sulfur compounds, *Carbon Energy*, 2024, **6**(2), e489.
28 M. Zielińska-Pisklak, P. Siekacz, Z. Stokłosa and Ł. Szeleszczuk, A Comprehensive Review of Substitutional Silicon-Doped C60 Fullerenes and Their Endohedral/Exohedral Complexes: Synthetic Strategies and Molecular Modeling Approaches, *Molecules*, 2025, **30**(19), 3912.
29 G. A. Okon, D. G. Malu, H. Y. Abdullah, C. R. Nwokoye, N. I. Gber and C. P. Egbo, *et al.*, Chalcogenides encapsulated Pt-doped carbon quantum dot (Pt@CQD) as a carrier for the controlled release of lapachone: Outlook from theoretical calculations, *Diamond Relat. Mater.*, 2024, **149**, 111628, DOI: 10.1016/j.diamond.2024.111628.
30 K. W. Qadir, M. D. Mohammadi and H. Y. Abdullah, Modelling gas adsorption onto Al12(Zn)N12 surfaces: A theoretical study of CH4, CO, CO2, H2O, N2, NH3, NO, NO2, O2, and SO2 interactions, *Comput. Theor. Chem.*, 2025, **1244**, 115063, DOI: 10.1016/j.comptc.2024.115063.
31 G. Yu, Y. Xie, Q. Ge, Q. Dai, J. Xu and H. Cao, Mechanism of ozone adsorption and activation on B-, N-, P-, and Si-doped graphene: A DFT study, *Chem. Eng. J.*, 2022, **430**, 133114, DOI: 10.1016/j.cej.2021.133114.
32 F. Behmagham, E. Vessally, B. Massoumi, A. Hosseinian and L. Edjlali, A computational study on the SO2 adsorption by the pristine, Al, and Si doped BN nanosheets, *Superlattices Microstruct.*, 2016, **100**, 350–357, DOI: 10.1016/j.spmi.2016.09.040.
33 B. O. Ekpong, H. Y. Abdullah, E. Emmanuel, I. Benjamin and D. C. Agurokpon, Transition metals tailoring of phosphorus-doped gallium nitride nanotubes as sensors for N-butenyl homoserine lactone (BHL): A computational study, *Comput. Theor. Chem.*, 2024, **1241**, 114914, DOI: 10.1016/j.comptc.2024.114914.
34 M. Doust Mohammadi, H. Y. Abdullah, H. Louis, E. E. Etim and H. O. Edet, Evaluating the detection potential of C59X fullerenes (X = C, Si, Ge, B, Al, Ga, N, P, and As) for H2SiCl2 molecule, *J. Mol. Liq.*, 2023, **387**, 122621, DOI: 10.1016/j.molliq.2023.122621.
35 Y. Liao, R. Peng, S. Peng, W. Zeng and Q. Zhou, The adsorption of h2 and c2h2 on ge-doped and cr-doped graphene structures: A DFT study, *Nanomaterials*, 2021, **11**(1), 231, DOI: 10.3390/nano11010231.
36 W. A. Mahdi, A. Alhowyan and A. J. Obaidullah, Computational study of carboplatin interaction with PEG-functionalized C60 fullerene as a drug carrier using DFT and molecular dynamics simulations, *Sci. Rep.*, 2025, **15**(1), 13707.
37 M. D. Esrafili and A. A. Khan, Alkali metal decorated C60fullerenes as promising materials for delivery of the 5-fluorouracil anticancer drug: A DFT approach, *RSC Adv.*, 2022, **12**(7), 3948–3956, DOI: 10.1039/d1ra09153k.
38 S. Bibi, S. Urrehman, L. Khalid, M. Yaseen, A. Q. Khan and R. Jia, Metal doped fullerene complexes as promising drug delivery materials against COVID-19, *Chem. Pap.*, 2021, **75**(12), 6487–6497, DOI: 10.1007/s11696-021-01815-4.
39 R. R. Panchuk, S. V. Prylutska, V. V. Chumak, N. R. Skorokhyd, L. V. Lehka and M. P. Evstigneev, *et al.*, Application of C60 fullerene-doxorubicin complex for tumor cell treatment in vitro and in vivo, *J. Biomed. Nanotechnol.*, 2015, **11**(7), 1139–1152.

40 L. M. Skivka, S. V. Prylutska, M. P. Rudyk, N. M. Khranovska, I. V. Opeida and V. V. Hurmach, *et al.*, C60 fullerene and its nanocomplexes with anticancer drugs modulate circulating phagocyte functions and dramatically increase ROS generation in transformed monocytes, *Cancer Nanotechnol.*, 2018, **9**(1), 8, DOI: 10.1186/s12645-017-0034-0.

41 W. M. Taha, M. Morsy, N. A. Nada and M. A. Ibrahim, Modeling the electronic properties for CNT interacted with ZnO, CuO, and Co3O4, *Opt. Quantum Electron.*, 2022, **54**(9), 597, DOI: 10.1007/s11082-022-03974-4.

42 M. Rezazade, S. Ketabi and M. Qomi, Effect of functionalization on the adsorption performance of carbon nanotube as a drug delivery system for imatinib: molecular simulation study, *BMC Chem.*, 2024, **18**(1), 85, DOI: 10.1186/s13065-024-01197-0.

43 M. D. Mohammadi, H. Y. Abdullah, H. Louis, E. E. Etim, H. O. Edet and O. C. Godfrey, Hexachlorobenzene (HCB) adsorption onto the surfaces of C60, C59Si, and C59Ge: Insight from DFT, QTAIM, and NCI, *Chem. Phys. Impact*, 2023, **6**, 100234, DOI: 10.1016/j.chphi.2023.100234.

44 H. Y. Abdullah, Theoretical study of the binding energy of some gases on Al-doped carbon nanotube, *Results Phys.*, 2016, **6**, 1146–1151, DOI: 10.1016/j.rinp.2016.11.053.

45 C. R. Girish, Determination of thermodynamic parameters in adsorption studies: a review, *Chem. Pap.*, 2025, **79**, 5687–5706, DOI: 10.1007/s11696-025-04218-x.

46 H. Jedli, C. Briki, A. Chrouda, J. Brahmi, A. Abassi and A. Jbara, *et al.*, Experimental and theoretical study of CO2 adsorption by activated clay using statistical physics modeling, *RSC Adv.*, 2019, **9**(66), 38454–38463, DOI: 10.1039/c9ra05904k.

47 A. D. Becke, Density-functional exchange-energy approximation with correct asymptotic behavior, *Phys. Rev. A: At., Mol., Opt. Phys.*, 1988, **38**(6), 3098.

48 M. Doust Mohammadi and H. Y. Abdullah, Non-covalent interactions of cysteine onto C60, C59Si, and C59Ge: a DFT study, *J. Mol. Model.*, 2021, **27**(11), 330, DOI: 10.1007/s00894-021-04960-5 PubMed PMID: 34709483.

49 Y. S. Al-Hamdani, M. Rossi, D. Alfe, T. Tsatsoulis, B. Ramberger and J. G. Brandenburg, *et al.*, Properties of the water to boron nitride interaction: From zero to two dimensions with benchmark accuracy, *J. Chem. Phys.*, 2017, **147**(4), 040901, DOI: 10.1063/1.4996116.

50 W. L. Yu, H. W. Zuo, C. H. Lu, Y. Li, Y. F. Zhang and W. K. Chen, Nitrous oxide decomposition catalyzed by Au19Pd and Au19Pt clusters, *Acta Phys.-Chim. Sin.*, 2015, **31**(3), 425–434, DOI: 10.3866/PKU.WHXB201501191.

51 P. Dhali and A. K. M. A. Hossain, Investigating the adsorption potential and sensitivity of pristine along with carbon, boron, and nitrogen substituted hetero-nanocages towards azacitidine drug, *J. Mol. Liq.*, 2024, **396**, 124051, DOI: 10.1016/j.molliq.2024.124051.

52 C. Lee, W. Yang and R. G. Parr, Development of the Colle-Salvetti correlation-energy formula into a functional of the electron density, *Phys. Rev. B: Condens. Matter Mater. Phys.*, 1988, **37**(2), 785, DOI: 10.1103/PhysRevB.37.785.

53 X. Min, W. Li, Z. Wei, R. Spinney, D. D. Dionysiou and Y. Seo, *et al.*, Sorption and biodegradation of pharmaceuticals in aerobic activated sludge system: a combined experimental and theoretical mechanistic study, *Chem. Eng. J.*, 2018, **342**, 211–219, DOI: 10.1016/j.cej.2018.01.012.

54 M. M. Aboelnga, J. J. Hayward and J. W. Gauld, Enzymatic post-transfer editing mechanism of E. coli threonyl-tRNA synthetase (ThrRS): A molecular dynamic (MD) and quantum mechanics/molecular mechanics (QM/MM) investigation, *ACS Catal.*, 2017, **7**(8), 5180–5193, DOI: 10.1021/acscatal.7b01554.

55 S. A. Elsayed, E. E. Saleh, M. M. Aboelnaga and E. A. Toson, Experimental and computational studies of silver(I) dibenzoylmethane-based complexes, interaction with DNA/RNA/BSA biomolecules, and in vitro cytotoxic activity, *J. Inorg. Biochem.*, 2023, **241**, 112132, DOI: 10.1016/j.jinorgbio.2023.112132 PubMed PMID: 36701985.

56 M. M. Aboelnga, Mechanistic insights into the chemistry of compound I formation in heme peroxidases: quantum chemical investigations of cytochrome *c* peroxidase, *RSC Adv.*, 2022, **12**(24), 15543–15554, DOI: 10.1039/d2ra01073a.

57 M. M. Aboelnga, M. M. Seliem, E. El-Bayoumy and M. El-Tahawy, DFT investigation of dye adsorption on pristine and doped graphdiyne: toward efficient removal of disperse yellow 3 from wastewater, *Nanoscale Adv.*, 2025, **7**(22), 7363–7381, DOI: 10.1039/d5na00720h.

58 A. Moumivand, F. Naderi, O. Moradi and B. Makiabadi, Smart drug delivery: a DFT study of C24 fullerene and doped analogs for pyrazinamide, *Nanoscale Adv.*, 2024, **7**(5), 1287–1299, DOI: 10.1039/d4na00560k.

59 K. Zare and N. Shadmani, Comparison of drug delivery systems: Nanotube and p-Sulphonatocalix [4] arene, by Density Functional Theory, *J. Nanostruct. Chem.*, 2013, **3**(1), 72.

60 M. D. Ganji, M. Nashtahosseini, S. Yeganegi and M. Rezvani, First-principles vdW-DF investigation on the interaction between the oxazepam molecule and C60 fullerene, *J. Mol. Model.*, 2013, **19**(4), 1929–1936, DOI: 10.1007/s00894-013-1758-3 PubMed PMID: 23344244.

61 V. Vetrivelan, S. Sakthivel, S. Muthu and A. A. Al-Saadi, Non-covalent interaction, adsorption characteristics and solvent effect of procainamide anti-arrhythmias drug on silver and gold loaded silica surfaces: SERS spectroscopy, density functional theory and molecular docking investigations, *RSC Adv.*, 2023, **13**(14), 9539–9554, DOI: 10.1039/d3ra00514c.

62 J. B. Pandya, P. D. Patel, S. M. Shinde and P. K. Jha, Interpreting the nature of interactions in the inclusion complex of danofloxacin, a third-generation fluoroquinolone with Cucurbit[7]uril: A computational study, *Comput. Theor. Chem.*, 2021, **1199**, 113210, DOI: 10.1016/j.comptc.2021.113210.

63 A. Shahali, M. Farahmand, H. A. Hussein, M. M. Kadhim, W. K. Abdelbasset and A. G. Ebadi, *et al.*, Quantum

chemical study the interaction between thiotepa drug and silicon doped graphdiyne, *Comput. Theor. Chem.*, 2022, **1209**, 113612, DOI: 10.1016/j.comptc.2022.113612.

64 F. Manouchehri and S. Iranpanah, Thioguanine adsorption on the γ-graphyne and its boron nitride analogue as promising drug delivery system: Electronic study *via* DFT, *Inorg. Chem. Commun.*, 2022, **144**, 109774, DOI: 10.1016/j.inoche.2022.109774.

65 M. Ishtiaq, M. U. Khan, A. Hamid, J. Yaqoob, R. Hussain and A. Ali, *et al.*, Systematic study of the structure-property relationship of C24N24 nanoclusters for the detection and electrochemical sensing of chemical warfare agents: molecular modelling at DFT level, *J. Mol. Struct.*, 2024, **1307**, 137905, DOI: 10.1016/j.molstruc.2024.137905.

66 Y. Li, Y. Xu and X. Li, The sensing mechanism of HCHO gas sensor based on transition metal doped graphene: Insights from DFT study, *Sens. Actuators, A*, 2022, **338**, 113460, DOI: 10.1016/j.sna.2022.113460.

67 E. D. Glendening, A. E. Reed, J. E. Carpenter and F. Weinhold, *NBO Version 3.1*, Gaussian Inc., Pittsburgh, PA, 2003.

68 R. A. Taha, A. S. Shalabi, M. M. Assem and K. A. Soliman, DFT study of adsorbing SO2, NO2, and NH3 gases based on pristine and carbon-doped Al24N24 nanocages, *J. Mol. Model.*, 2023, **29**(5), 140, DOI: 10.1007/s00894-023-05547-y PubMed PMID: 37059860.

69 J. Panchal, A. Gauswami, D. Chodvadiya, H. Jadeja and P. K. Jha, Adsorption performance of CO, NO and NH3 hazardous gas molecules over B9N9 and Al9N9 nanorings: Acumen from density functional theory, *Mater. Chem. Phys.*, 2024, **311**, 128565, DOI: 10.1016/j.matchemphys.2023.128565.

70 H. Wang, L. Yu, J. Xu, D. Wei, G. Qin and Y. Yao, *et al.*, Intrinsically low lattice thermal conductivity of monolayer hexagonal aluminum nitride (h-AlN) from first-principles: A comparative study with graphene, *Int. J. Therm. Sci.*, 2021, **162**, 106772.

71 R. Sainda, D. Chodvadiya, I. Zgłobicka, K. J. Kurzydłowski and P. K. Jha, The First-Principles investigation of sensing and removal applications of nitrobenzene using pristine and Sc decorated B9N9 nanoring, *J. Mol. Liq.*, 2024, **409**, 125389, DOI: 10.1016/j.molliq.2024.125389.

72 F. M. A. Altalbawy, U. A. R. Hussein, I. S. Alalaq, I. Kaur, A. Kumar and M. Chahar, *et al.*, Computational investigation of pristine, Al-, and Ga-doped Zn12O12 nanoclusters as detection platforms for methadone in gas and solvent phases, *J. Organomet. Chem.*, 2025, 1025, DOI: 10.1016/j.jorganchem.2024.123469.

73 H. Sajid, K. Ayub and T. Mahmood, Sensing behaviour of monocyclic C18 and B9N9 analogues toward chemical warfare agents (CWAs); quantum chemical approach, *Surf. Interfaces*, 2022, **30**, 101912, DOI: 10.1016/j.surfin.2022.101912.

74 C. Zhang and M. Derakhshandeh, CS2 adsorption on pristine and Al-doped graphynes: A DFT study, *Comput. Theor. Chem.*, 2021, **1204**, 113380.

75 H. Ji, T. Wang, T. Huang, B. Lai and W. Liu, Adsorptive removal of ciprofloxacin with different dissociated species onto titanate nanotubes, *J. Cleaner Prod.*, 2021, **278**, 123924.

76 A. M. Aljeboree, N. D. Radia, L. S. Jasim, A. A. Alwarthan, M. M. Khadhim and A. W. Salman, *et al.*, Synthesis of a new nanocomposite with the core TiO2/hydrogel: Brilliant green dye adsorption, isotherms, kinetics, and DFT studies, *J. Ind. Eng. Chem.*, 2022, **109**, 475–485.

77 Y. Du, H. Che, P. Wang, J. Chen and Y. Ao, Highly efficient removal of organic contaminant with wide concentration range by a novel self-cleaning hydrogel: Mechanism, degradation pathway and DFT calculation, *J. Hazard. Mater.*, 2022, **440**, 129738.

78 H. Wang, X. Li, J. Li, Z. Xie and G. Chang, Synthesis of a ''Turn-On'' Mg2+ fluorescent probe and its application in hydrogel adsorption, *J. Mol. Struct.*, 2023, **1281**, 135085.

79 L. Jayarathna, A. Bandara, W. J. Ng and R. Weerasooriya, Fluoride adsorption on γ-Fe 2 O 3 nanoparticles, *J. Environ. Health Sci. Eng.*, 2015, **13**, 1–10.

80 Q. Shi, L. Yan, T. Chan and C. Jing, Arsenic adsorption on lanthanum-impregnated activated alumina: spectroscopic and DFT study, *ACS Appl. Mater. Interfaces*, 2015, **7**(48), 26735–26741.

81 T. N. V. de Souza, S. M. L. de Carvalho, M. G. A. Vieira, M. G. C. da Silva and D. D. S. B. Brasil, Adsorption of basic dyes onto activated carbon: experimental and theoretical investigation of chemical reactivity of basic dyes using DFT-based descriptors, *Appl. Surf. Sci.*, 2018, **448**, 662–670.

82 R. El Haouti, H. Ouachtak, A. El Guerdaoui, A. Amedlous, E. Amaterz and R. Haounati, *et al.*, Cationic dyes adsorption by Na-Montmorillonite Nano Clay: Experimental study combined with a theoretical investigation using DFT-based descriptors and molecular dynamics simulations, *J. Mol. Liq.*, 2019, **290**, 111139.

83 J. R. de Andrade, M. F. Oliveira, R. L. S. Canevesi, R. Landers, M. G. C. da Silva and M. G. A. Vieira, Comparative adsorption of diclofenac sodium and losartan potassium in organophilic clay-packed fixed-bed: X-ray photoelectron spectroscopy characterization, experimental tests and theoretical study on DFT-based chemical descriptors, *J. Mol. Liq.*, 2020, **312**, 113427.

84 M. H. Abdel-Aziz, E. Z. El-Ashtoukhy, M. Bassyouni, A. F. Al-Hossainy, E. M. Fawzy and S. M. S. Abdel-Hamid, *et al.*, DFT and experimental study on adsorption of dyes on activated carbon prepared from apple leaves, *Carbon Lett.*, 2021, **31**, 863–878.

85 M. P. Spaolonzi, M. G. C. da Silva and M. G. A. Vieira, Adsorption of antibiotic cefazolin in organoclay fixed-bed column: characterization, mathematical modeling, and DFT-based calculations, *Environ. Sci. Pollut. Res.*, 2022, **29**(21), 31646–31658.

86 G. Abdollahizad, F. M. Valadi, E. Akbarzadeh and M. R. Gholami, Adsorption properties of halloysite modified acrylamide/quince seeds-based hydrogel: Experimental and DFT investigation, *J. Polym. Environ.*, 2022, **30**(11), 4637–4650.

87 M. D. Esrafili and A. A. Khan, Alkali metal decorated C60fullerenes as promising materials for delivery of the 5-fluorouracil anticancer drug: A DFT approach, *RSC Adv.*, 2022, **12**(7), 3948–3956, DOI: 10.1039/d1ra09153k.

88 A. Hosseinian, E. Vessally, S. Yahyaei, L. Edjlali and A. Bekhradnia, A Density Functional Theory Study on the Interaction Between 5-Fluorouracil Drug and C24 Fullerene, *J. Cluster Sci.*, 2017, **28**(5), 2681–2692, DOI: 10.1007/s10876-017-1253-6.

89 M. A. Alkhalifah, M. Yar, I. Bayach, N. S. Sheikh and K. Ayub, Covalent organic framework (C6N6) as a drug delivery platform for fluorouracil to treat cancerous cells: a DFT study, *Materials*, 2022, **15**(21), 7425, DOI: 10.3390/ma15217425.

90 M. K. Hazrati, Z. Bagheri and A. Bodaghi, Application of C30B15N15 heterofullerene in the isoniazid drug delivery: DFT studies, *Phys. E*, 2017, **89**, 72–76, DOI: 10.1016/j.physe.2017.02.009.

91 E. Alipour, F. Alimohammady, A. Yumashev and A. Maseleno, Fullerene C60 containing porphyrin-like metal center as drug delivery system for ibuprofen drug, *J. Mol. Model.*, 2020, **26**(1), 7, DOI: 10.1007/s00894-019-4267-1 PubMed PMID: 31834504.

92 F. Nattagh, S. Hosseini and M. D. Esrafili, Effects of B and N doping/codoping on the adsorption behavior of C60 fullerene towards aspirin: A DFT investigation, *J. Mol. Liq.*, 2021, **342**, 117459, DOI: 10.1016/j.molliq.2021.117459.

93 H. Hadi, C. H. Lai, D. C. Agurokpon, H. C. B. de Oliveira and H. Louis, The effect of chemically functionalized C60-nanocages as sorbents and sensors for methamphetamine drug: A DFT and QTAIM study, *Diamond Relat. Mater.*, 2024, **141**, 110722, DOI: 10.1016/j.diamond.2023.110722.

94 M. Reza, J. Sarvestani and S. A. Majedi, DFT study on the interaction of alprazolam with fullerene (C20), *J. Chem. Lett.*, 2020, **1**, 32–38, DOI: 10.22034/jchemlett.2020.108111.

95 M. H. Fekri, R. Bazvand, M. Soleymani and M. M. Razavi, Adsorption of Metronidazole drug on the surface of nano fullerene C60 doped with Si, B and Al: A DFT study, *Int. J. Nano Dimens.*, 2020, **11**(4), 346–354.

96 F. Kamali, G. Ebrahimzadeh Rajaei, S. Mohajeri, A. Shamel and M. Khodadadi-Moghaddam, Adsorption behavior of metformin drug on the C60 and C48 nanoclusters: a comparative DFT study, *Monatsh. Chem.*, 2020, **151**(5), 711–720, DOI: 10.1007/s00706-020-02597-3.

97 W. A. Mahdi, A. Alhowyan and A. J. Obaidullah, Computational study of carboplatin interaction with PEG-functionalized C60 fullerene as a drug carrier using DFT and molecular dynamics simulations, *Sci. Rep.*, 2025, **15**(1), 13707, DOI: 10.1038/s41598-025-98262-y PubMed PMID: 40258912.

98 M. A. S. Sakr, H. Abdelsalam, N. H. Teleb, M. A. Saad, O. H. Abd-Elkader and Y. Liu, *et al.*, Exploring the drug delivery capabilities of Nb2C MXene functionalized with oxygen and fluorine: A DFT study, *J. Mol. Graphics Modell.*, 2025, **136**, 108937, DOI: 10.1016/j.jmgm.2024.108937 PubMed PMID: 39756354.

99 A. U. Rahman, M. K. Rokunuzzaman, D. M. Saaduzzaman, M. S. Rahman, M. Amin and S. M. Hasan, *et al.*, Designing nitride-derived fullerenes X 20 N 20 (X= B, Al, and Ga) for the effective delivery of the cardiovascular drug felodipine: a DFT study, *Nanoscale*, 2025, **17**(42), 24755–24772.

100 A. M. Khudhair and A. Ben Ahmed, Anticancer drugs delivery and adsorption computations in pure and Stone–Wales defect armchair graphene nanoribbons, *Opt. Quantum Electron.*, 2023, **55**(9), 812.